Ab initio thermodynamic and elastic properties of $AGaH_4$ hydrides (A=Li, Na, K, Rb, and Cs)

J. F. Herbst and L. G. Hector, Jr.
Chemical Sciences and Materials Systems Laboratory, GM R&D Center, Mail Code 480-106-224, 30500 Mound Road, Warren, Michigan 48090-9055, USA

W. Wolf
Materials Design, P.O. Box 2000, Angel Fire, New Mexico 87710, USA

(Received 18 May 2010; revised manuscript received 24 June 2010; published 27 July 2010)

Systematic properties of the $AGaH_4$ alkali gallium hydrides (A=Li, Na, K, Rb, and Cs) are investigated within density functional theory. Seven ground-state crystal structures are identified, with two energetically indistinguishable structures found for both $LiGaH_4$, whose structure is as yet undetermined experimentally, and $CsGaH_4$. Born effective charge tensors, static and high-frequency dielectric tensors, and phonon dispersion relations incorporating longitudinal-optical/transverse-optical mode splittings are computed. Our results indicate that $LiGaH_4$ and $NaGaH_4$ have technologically interesting standard enthalpies of formation near −30 kJ/mole H_2. We find, however, that $LiGaH_4$ is thermodynamically unstable with respect to both LiGa and LiH, providing a possible explanation for its challenging synthesis. The Born stability criteria are evaluated with the computed elasticity tensor components, C_{ij}. All seven structures are found to be both elastically and vibrationally stable.

DOI: 10.1103/PhysRevB.82.024110 PACS number(s): 61.50.Ah, 61.50.Lt, 63.20.−e

I. INTRODUCTION

Alkali-containing ternary hydrides such as $LiBH_4$, $LiAlH_4$, $NaBH_4$, and $NaAlH_4$ have been studied extensively as potential hydrogen storage media in view of their substantial hydrogen gravimetric density.[1–6] In addition to their intrinsic scientific interest, the ongoing technological need for efficient methods of hydrogen storage in mobile applications, fuel cell vehicles in particular, makes this genre of materials worthy of continued investigation. Here we report a systematic theoretical study of the $AGaH_4$ series (A=Li, Na, K, Rb, and Cs) with isoelectronic Ga in place of B or Al. Investigation of an entire group of cognate materials affords identification of property trends, as we demonstrated previously in comprehensive work on the alkaline-earth metals and their hydrides.[7]

We examine several distinct model crystal structures, including those known from experiment for the A=Na, K, Rb, and Cs hydrides, in order to (1) identify a candidate ground-state structure for $LiGaH_4$ and (2) determine if energetically comparable alternatives exist for all the compounds. Vajeeston *et al.*[8] pursued a similar approach, comparing the electronic total energies of various models to find the most thermodynamically stable structure for each $AGaH_4$. In contrast to Ref. 8, we identify two energetically indistinguishable possible ground-state structures for $LiGaH_4$ and for $CsGaH_4$. We go beyond the electronic contributions to calculate dielectric properties [Born effective charge tensor (BECT) and dielectric tensors], phonon spectra with inclusion of the longitudinal- and transverse-optical (LO/TO) zone-center splittings, enthalpies of formation at zero temperature and 298 K, the components of the elasticity tensor C_{ij}, and Voigt-Reuss-Hill polycrystalline moduli. Elastic stability is examined with the methods we applied previously to LiH, $LiNH_2$, and Li_2NH.[9] Comparison is made with available thermodynamic measurements.

II. COMPUTATIONAL METHODS

All calculations in this work are based on density functional theory[10] (DFT) as implemented in the Vienna *ab initio* simulation package (VASP) within a plane-wave basis set.[11,12] Potentials constructed by the projector-augmented wave (PAW) method were employed for the elements;[13,14] the generalized gradient approximation of Perdew and Wang[15,16] in conjunction with the interpolation formula of Vosko *et al.*[17] was used for the exchange-correlation energy functional. The plane-wave cutoff energies of the PAW potentials for Li, Na, K, Rb, Cs, Ga, and H were 271.798 eV, 300.000 eV, 150.000 eV, 220.155 eV, 220.143 eV, 282.718 eV, and 700.000 eV, respectively; a particularly hard PAW was chosen for hydrogen to achieve high accuracy. For Ga semicore d electrons, for Na and K semicore p states, for Rb and Cs semicore s and p states, and for Li all electrons were included in the variational self-consistent field procedures. Lattice constants and atomic positions were optimized by simultaneously minimizing all atomic forces and stress tensor components via a conjugate gradient method.[18] Monkhorst-Pack reciprocal space meshes[19] having k-point spacings no larger than 0.14 $Å^{-1}$ were used; for the most stable structures, in particular, the spacings were in the 0.04–0.09 $Å^{-1}$ range to ensure precise electronic total energies. In all calculations the plane-wave cutoff energy was 900 eV (much larger than any of the potential cutoff energies), the total energy was converged to 10^{-6} eV per cell, and the force components relaxed to at least 10^{-4} eV/Å. No fewer than three successive full-cell optimizations were conducted to ensure that the structural parameters and cell energies were fully converged. Total energies were derived by integration over the irreducible Brillouin zone with the linear tetrahedron method including Blöchl corrections.[20] The energy of the H_2 molecule was computed with the same 900 eV plane-wave cutoff in a $12\times13\times14$ $Å^3$ orthorhombic box large enough to guarantee isolation from periodic images.

TABLE I. Structural parameters for the most stable $A\mathrm{GaH_4}$ structures. Lattice constants a, b, c in Å; cell volumes V in $\mathrm{Å^3/f.u.}$; and atomic positions in fractions of the lattice vectors of the conventional cell.

Hydride (space group)	Lattice constants	Atomic positions
$\mathrm{LiGaH_4}$ ($P2_1/c$)	a: 4.8736	Li $4e$:(0.0689 0.0384 0.1760)
	b: 7.8523	Ga $4e$:(0.2920 0.7049 0.9323)
	c: 9.9352	H $4e_1$:(0.3475 0.3950 0.2307)
	β: 48.05°	H $4e_2$:(0.5889 0.1255 0.0240)
	V: 70.699	H $4e_3$:(0.0395 0.5900 0.1083)
		H $4e_4$:(0.0668 0.7620 0.8762)
$\mathrm{LiGaH_4}$ ($Cmcm$)	a: 6.4751	Li $4c$:(0 0.4246 $\frac{1}{4}$)
	6.5275[a]	(0 0.4260 $\frac{1}{4}$) [a]
	b: 7.0749	Ga $4c$:(0 −0.1826 $\frac{1}{4}$)
	7.0384[a]	(0 −0.1783 $\frac{1}{4}$) [a]
	c: 6.1639	H $8f$:(0 0.6729 0.4519)
	6.2093[a]	(0 0.6740 0.4536)[a]
	V: 70.593	H $8g$:(0.2003 −0.0555 $\frac{1}{4}$)
	71.319[a]	(0.1799 −0.0486 $\frac{1}{4}$) [a]
$\mathrm{NaGaH_4}$ ($Cmcm$)	a: 7.0662	Na $4c$:(0 0.3438 $\frac{1}{4}$)
	7.1102[a]	(0 0.3439 $\frac{1}{4}$) [a]
	7.060[b], 7.105[c]	(0 0.350 $\frac{1}{4}$) [b]
	b: 6.4163	Ga $4c$:(0 −0.1595 $\frac{1}{4}$)
	6.4717[a]	(0 −0.1599 $\frac{1}{4}$) [a]
	6.482[b], 6.637[c]	(0 −0.162 $\frac{1}{4}$) [b]
	c: 7.1387	H $8f$:(0 0.6911 0.4286)
	7.1089[a]	(0 0.6879 0.4313)[a]
	7.060[b], 7.102[c]	(0 0.686 0.428)[b]
	V: 80.916	H $8g$:(0.1827 −0.0134 $\frac{1}{4}$)
	81.779[a]	(0.1409 −0.0109 $\frac{1}{4}$) [a]
	80.77[b], 83.73[c]	(0.187 −0.012 $\frac{1}{4}$) [b]
$\mathrm{KGaH_4}$ ($Pnma$)	a: 9.0956	
	9.1133[a]	K $4c$:(0.1814 $\frac{1}{4}$ 0.1618)
	9.10[c]	(0.1806 $\frac{1}{4}$ 0.1616) [a]
	b: 5.6185	Ga $4c$:(0.5628 $\frac{1}{4}$ 0.8091)
	5.6467[a]	(0.5632 $\frac{1}{4}$ 0.8096) [a]
	5.69[c]	H $4c_1$:(0.4019 $\frac{1}{4}$ 0.8928)
	c: 7.3604	(0.3990 $\frac{1}{4}$ 0.8951) [a]
	7.3990[a]	H $4c_2$:(0.6890 $\frac{1}{4}$ 0.9590)
	7.38[c]	(0.6939 $\frac{1}{4}$ 0.9620) [a]
	V: 94.036	H $8d$:(0.4167 0.9802 0.3178)
	95.188[a]	(0.4119 0.9862 0.3197)[a]
	95.5[c]	

TABLE I. (*Continued.*)

Hydride (space group)	Lattice constants	Atomic positions
$RbGaH_4$ (*Pnma*)	*a*: 9.4928	
	9.5390[a]	Rb $4c$:(0.1824 $\frac{1}{4}$ 0.1624)
	9.42[c]	(0.1781 $\frac{1}{4}$ 0.1689) [a]
	b: 5.7726	Ga $4c$:(0.5621 $\frac{1}{4}$ 0.8071)
	5.8275[a]	(0.5681 $\frac{1}{4}$ 0.8095) [a]
	5.801[c]	H $4c_1$:(0.4077 $\frac{1}{4}$ 0.8879)
	c: 7.6179	(0.4112 $\frac{1}{4}$ 0.9122) [a]
	7.6823[a]	H $4c_2$:(0.6827 $\frac{1}{4}$ 0.9528)
	7.54[c]	(0.7081 $\frac{1}{4}$ 0.9483) [a]
	V: 104.36	H $8d$:(0.4178 0.9740 0.3154)
	106.76[a]	(0.4165 0.9810 0.3231)[a]
	103[c]	
$CsGaH_4$ (*Pnma*)	*a*: 10.0399	
	10.0154[a]	Cs $4c$:(0.1845 $\frac{1}{4}$ 0.1642)
	9.90[c], 9.90[d]	(0.1794 $\frac{1}{4}$ 0.1653) [a]
	b: 5.9992	Ga $4c$:(0.5600 $\frac{1}{4}$ 0.8038)
	6.0995[a]	(0.5652 $\frac{1}{4}$ 0.8076) [a]
	5.98[c], 5.93[d]	H $4c_1$:(0.4138 $\frac{1}{4}$ 0.8810)
	c: 7.9668	(0.4025 $\frac{1}{4}$ 0.8970) [a]
	7.9831[a]	H $4c_2$:(0.6735 $\frac{1}{4}$ 0.9441)
	7.82[c], 7.82[d]	(0.6994 $\frac{1}{4}$ 0.9526) [a]
	V: 119.96	H $8d$:(0.4205 0.9657 0.3132)
	121.92[a]	(0.4163 0.9796 0.3229)[a]
	116[c]	
$CsGaH_4$ ($P4_2/nmc$)	*a*: 5.6368	Cs $2a$:($\frac{3}{4}$ $\frac{1}{4}$ $\frac{3}{4}$)
	c: 7.8738	Ga $2b$:($\frac{3}{4}$ $\frac{1}{4}$ $\frac{1}{4}$)
	V: 125.09	H $8g$:($\frac{1}{4}$ 0.5185 0.8673)

[a]Reference 8 (DFT).
[b]Reference 30 (experiment, 80 K).
[c]Reference 31 (experiment).
[d]Reference 33 (experiment).

Phonon spectra for the solids, the vibrational frequency of the H_2 molecule, and the thermodynamic functions were computed by means of the direct approach to lattice dynamics,[21–23] with VASP as the computational engine. The direct method involves construction of $N+1$ supercells: an unperturbed supercell and N perturbed supercells, where N is the number of crystallographically independent displacements of the constituent atoms. In each perturbed supercell, a single atom is displaced in a Cartesian direction in such a way that the N supercells explore all the degrees of freedom of each symmetry-unique atomic site. Atomic displacements of ± 0.02 Å were applied to evaluate the resulting force constants within a harmonic response; both smaller and larger displacements were also tested and found to have no effect on the results. The supercell size was chosen such that interactions between equivalent atoms in periodic images were negligible, as were the computed force constants at the boundaries of each supercell. For each of the $N+1$ supercells the forces on all atoms were computed with VASP. Reciprocal space integration was performed by means of the Methfessel-Paxton technique[24] with a smearing width of 0.1 eV (the phonon results showed no sensitivity to small deviations in smearing width above and below 0.1 eV). From the *ab initio* forces obtained from each supercell, the force constant matrices were computed through a least-squares fit to the equations of motion of the lattice within the harmonic approxi-

TABLE II. Ga-H nearest-neighbor distances d(Ga-H), H-Ga-H bond angle ranges, and energy gaps E_g for the most stable AGaH$_4$ crystal structures.

Hydride (space group)	d(Ga-H) (Å)	∠H-Ga-H	E_g (eV)
LiGaH$_4$ ($P2_1/c$)	1.584–1.623	108.4°–111.0°	4.46
LiGaH$_4$ ($Cmcm$)	1.579–1.611	101.2°–111.2°	4.64
NaGaH$_4$ ($Cmcm$)	1.595–1.596	106.1°–110.7°	4.73
KGaH$_4$ ($Pnma$)	1.588–1.606	107.3°–113.3°	4.94
RbGaH$_4$ ($Pnma$)	1.589–1.606	107.2°–113.1°	4.94
CsGaH$_4$ ($Pnma$)	1.592–1.607	107.3°–112.8°	4.99
CsGaH$_4$ ($P4_2/nmc$)	1.599	109.4°–109.5°	4.71

mation. Fourier transformation of the force constants yielded the dynamical matrix, diagonalization of which provided phonon frequencies and eigenvalues for each selected q-point in reciprocal space. Integration over a large sample of q vectors in the entire Brillouin zone yielded the phonon density of states (DOS) from which the thermodynamic functions were computed. The force constants for each calculation were carefully examined to ensure that they became vanishingly small a few angstroms from each symmetry-unique displacement site so that the point at which the force constants vanished was well within the boundaries of the corresponding supercell. The vibrational frequency of H_2 was computed with the same machinery.

Ion core displacement in insulating ionic crystals such as the AGaH$_4$ hydrides may create a macroscopic electric field that splits LO and TO phonon modes in the neighborhood of the Γ-point in the Brillouin zone. The field breaks the crystal symmetry so that the LO/TO mode splittings cannot be computed by the direct approach based on supercells. The corresponding nonanalytic term in the dynamical matrix is taken into account, however, by making use of the high-frequency dielectric tensor and the BECT which describes the coupling between optical phonons and the electric field responsible for the splittings.[25] We compute these tensors explicitly for the seven most stable AGaH$_4$ structures. Thermodynamic quantities derived from integration of the phonon energies over the entire Brillouin zone [e. g., zero-point energy (ZPE), finite-temperature phonon energy] are not expected to be significantly affected by the LO/TO mode splitting. Thermal-expansion effects and the volume dependence of the zero-point energy, anticipated to be negligible, are ignored.

We calculated the elasticity tensor, C_{ij}, with the stress-based least-squares fitting method of LePage and Saxe[26] that we applied previously to other hydrides.[27,28] The method relies on the stresses computed in VASP as inputs to a least-squares fit of the unknowns appearing in the equations describing the linear stress-strain relationships for a selected sequence of strains applied in various directions. The unknowns are the 6, 9, and 13 independent C_{ij} for the tetragonal, orthorhombic, and monoclinic symmetries of the AGaH$_4$ structures investigated here. The moduli are computed from the first derivatives of the stresses with respect to strain rather than from the second derivatives of the total energy with respect to strain. In this way the method circumvents

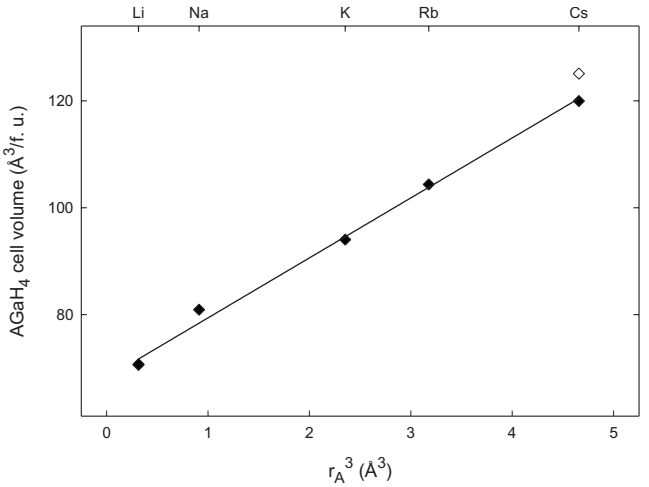

FIG. 1. AGaH$_4$ cell volume (Å^3/f.u.) vs r_A^3, where r_A is radius of the alkali ion A^{+1}. The open symbol is for the $P4_2/nmc$ CsGaH$_4$ structure. The line is a fit to the filled symbols only.

the numerical difficulties often encountered with evaluation of the latter, and individual C_{ij}, rather than various sums of them, are computed.[29] Perhaps the most advantageous feature of the method, however, is its full exploitation of symmetry which makes for optimum computational efficiency. Tests were conducted with selected strains to determine the total number necessary to minimize the least-squares errors for each C_{ij}. It was determined that application of six suc-

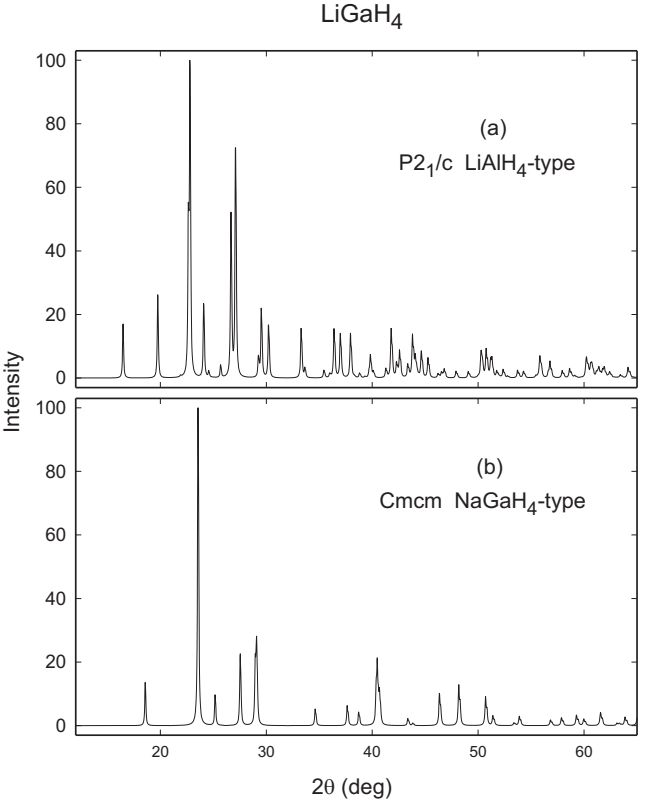

FIG. 2. Cu K_α powder diffraction diagrams calculated for LiGaH$_4$ in the (a) monoclinic $P2_1/c$ LiAlH$_4$-type structure and the (b) orthorhombic $Cmcm$ NaGaH$_4$-type structure.

TABLE III. Components of the high-frequency $[\varepsilon_{\alpha\beta}(\infty)]$ and static $[\varepsilon_{\alpha\beta}(0)]$ dielectric tensors for the most stable $A\mathrm{GaH_4}$ hydrides.

	$\varepsilon_{\alpha\beta}(\infty)$				$\varepsilon_{\alpha\beta}(0)$			
Hydride (space group)	*xx*	*yy*	*zz*	*xz=zx*	*xx*	*yy*	*zz*	*xz=zx*
$LiGaH_4$ ($P2_1/c$)	3.42	3.47	3.33	−0.06	8.76	8.52	8.49	−0.33
$LiGaH_4$ (*Cmcm*)	3.15	3.25	3.07		6.69	7.08	7.63	
$NaGaH_4$ (*Cmcm*)	2.90	2.99	2.84		8.27	7.55	5.81	
$KGaH_4$ (*Pnma*)	2.92	2.95	2.90		6.16	8.26	6.07	
$RbGaH_4$ (*Pnma*)	2.82	2.82	2.79		5.92	7.01	5.51	
$CsGaH_4$ (*Pnma*)	2.80	2.79	2.77		5.71	6.36	5.42	
$CsGaH_4$ ($P4_2/nmc$)	2.56	=*xx*	2.54		5.59	=*xx*	5.11	

cessive strains, viz., 0.5%, 0.6%, 0.7%, 0.8%, 0.9%, and 1.0%, was adequate to obtain ≤1% statistical error in each C_{ij}. In addition, the quality of the least-squares fit, as measured by the computed least-squares residual, was ≤1% for all elastic constant calculations. The small residuals indicate that anharmonic effects due to the applied strains are negligible. Tests with additional intermediate strains showed no significant deviation from the results reported here. Separate calculations with different *k*-point meshes were also conducted to determine the meshes needed to converge each C_{ij} to ≤0.5 GPa.

III. CRYSTAL STRUCTURES AND LATTICE OPTIMIZATION

Orthorhombic structures have been documented in the literature for $NaGaH_4$ (*Cmcm*, space group No. 63)[30–32] and for $KGaH_4$, $RbGaH_4$, and $CsGaH_4$ ($BaSO_4$-type, *Pnma*, No. 62).[31,33] There is experimental evidence that $LiGaH_4$ forms,[34,35] albeit with considerable difficulty, but the literature is silent regarding its detailed structure. For each $A\mathrm{GaH_4}$ hydride we investigated a total of eight prototype structures, the two known and six others: (i) $LiAlH_4$ (monoclinic, $P2_1/c$, No. 14); (ii) $NaAlH_4$ (tetragonal, $I4_1/a$, No. 88); (iii) $LiBH_4$ (hexagonal, $P6_3mc$, No. 186); (iv) $NaBD_4$ (tetragonal, $P\bar{4}2_1c$; No. 114);[36] (v) $NaBD_4$ (tetragonal, $P4_2/nmc$, No. 137);[37] and (vi) $SrMgH_4$ (orthorhombic, $Cmc2_1$, No. 36; Sr→Li, Mg→Ga). Vajeeston *et al.*[8] considered a similar set of seven models that included an ordered variant of the $NaBH_4$ structure (cubic, $F\bar{4}3m$, No. 216) but not (iv) and (v). It is challenging to determine a precise crystal structure from first-principles calculations, and several methods for doing so, including database mining, simulated annealing, modified cluster expansion,[38] potential basin hopping,[39] and genetic algorithm,[40] have been reported in the literature. Our approach here is a limited database search confined to chemically similar materials that we believe is sufficient to yield a reasonably accurate ground state energy for $LiGaH_4$ if not the actual structure.

The electronic total energies E_{el} from the VASP optimizations for $NaGaH_4$, $KGaH_4$, and $RbGaH_4$ indicate that the observed structures are indeed the most thermodynamically stable, with E_{el} for the seven other candidates higher in each case by at least 0.01 eV per $A\mathrm{GaH_4}$ formula unit (f.u.), which

TABLE IV. Components of the Born effective charge tensor $Z^*_{\tau,\alpha\beta}$ for the orthorhombic *Cmcm* structures of $LiGaH_4$ and $NaGaH_4$.

	$Z^*_{\tau,\alpha\beta}$						
Atom τ	*xx*	*yy*	*zz*	*xy*	*yx*	*yz*	*zy*
			$LiGaH_4$ (*Cmcm*)				
Li 4*c*	1.26	1.07	1.18				
Ga 4*c*	1.38	1.52	1.42				
H 8*f*	−0.43	−0.76	−0.87			0.20	0.28
H 8*g*	−0.89	−0.54	−0.42	0.17	0.22		
			$NaGaH_4$ (*Cmcm*)				
Na 4*c*	1.15	1.25	1.12				
Ga 4*c*	1.24	1.24	1.31				
H 8*f*	−0.43	−0.63	−0.82			0.18	0.22
H 8*g*	−0.76	−0.61	−0.39	−0.16	−0.17		

TABLE V. Components of the Born effective charge tensor $Z^*_{\tau,\alpha\beta}$ for the monoclinic $P2_1/c$ structure of $LiGaH_4$ and the orthorhombic *Pnma* structures of $KGaH_4$, $RbGaH_4$, and $CsGaH_4$.

	$Z^*_{\tau,\alpha\beta}$								
Atom τ	*xx*	*yy*	*zz*	*xy*	*yx*	*xz*	*zx*	*yz*	*zy*
				$LiGaH_4$ ($P2_1/c$)					
Li $4e$	1.12	1.16	1.11	−0.07	0.16	0.02	−0.02	0.05	−0.10
Ga $4e$	1.54	1.63	1.55	0.16	0.14	−0.11	−0.08	0.00	−0.01
H $4e_1$	−0.61	−0.60	−0.75	0.11	0.12	0.20	0.23	−0.16	−0.20
H $4e_2$	−0.71	−0.90	−0.60	−0.29	−0.30	0.02	0.04	−0.13	−0.08
H $4e_3$	−0.48	−0.65	−0.83	−0.06	−0.02	0.00	−0.05	0.26	0.19
H $4e_4$	−0.84	−0.62	−0.46	0.15	0.10	−0.14	−0.13	0.03	0.07
				$KGaH_4$ (*Pnma*)					
K $4c$	1.15	1.16	1.15			−0.12	−0.09		
Ga $4c$	1.21	1.23	1.20			−0.11	−0.03		
H $4c_1$	−0.78	−0.46	−0.51			0.18	0.16		
H $4c_2$	−0.63	−0.48	−0.62			−0.14	−0.19		
H $8d$	−0.47	−0.72	−0.60	0.03	0.02	0.05	0.02	−0.20	−0.18
				$RbGaH_4$ (*Pnma*)					
Rb $4c$	1.18	1.18	1.16			−0.11	−0.07		
Ga $4c$	1.19	1.21	1.18			−0.09	−0.02		
H $4c_1$	−0.78	−0.45	−0.49			0.16	0.16		
H $4c_2$	−0.63	−0.48	−0.64			−0.16	−0.21		
H $8d$	−0.47	−0.73	−0.59	0.03	0.03	0.05	0.03	−0.20	−0.18
				$CsGaH_4$ (*Pnma*)					
Cs $4c$	1.25	1.24	1.21			−0.09	−0.06		
Ga $4c$	1.19	1.21	1.17			−0.07	0.00		
H $4c_1$	−0.80	−0.45	−0.49			0.16	0.16		
H $4c_2$	−0.64	−0.49	−0.66			−0.18	−0.22		
H $8d$	−0.50	−0.74	−0.61	0.03	0.03	0.05	0.03	−0.20	−0.18

we believe is the reliable limit of precision for VASP. Two structures with E_{el} values separated by less than 0.002 eV/f.u., and hence computationally indistinguishable, were found for A=Li and Cs. For $LiGaH_4$ these are the orthorhombic *Cmcm* $NaGaH_4$-type (E_{el}=−19.0577 eV/f.u.) and the monoclinic $P2_1/c$ $LiAlH_4$-type (E_{el}=−19.0561 eV/f.u.), and for $CsGaH_4$ the orthorhombic *Pnma* $KGaH_4$-type (E_{el} =−18.6851 eV/f.u.), the structure reported by Kovba *et al.*[31] and by Dymova and Dergachev,[33] and the tetragonal $P4_2/nmc$ $NaBD_4$-type (E_{el}=−18.6834 eV/f.u.). Vajeeston *et al.*[8] found the *Cmcm* (*Pnma*) structures to be the most stable for A=Li and Na (K, Rb, and Cs). Table I lists the lattice

TABLE VI. Components of the Born effective charge tensor $Z^*_{\tau,\alpha\beta}$ for the tetragonal $P4_2/nmc$ structure of $CsGaH_4$.

	$CsGaH_4$ ($P4_2/nmc$) $Z^*_{\tau,\alpha\beta}$				
Atom τ	*xx*	*yy*	*zz*	*yz*	*zy*
Cs $2a$	1.21	=*xx*	1.23		
Ga $2b$	1.10	=*xx*	1.07		
H $8g$	−0.45	−0.70	−0.57	0.18	0.16

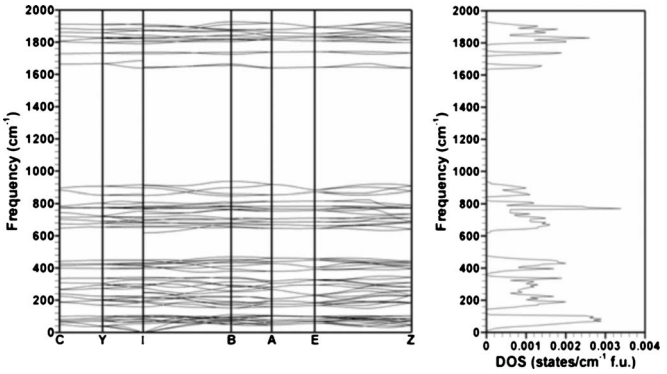

FIG. 3. Phonon spectrum and corresponding density of states (DOS) for the monoclinic $P2_1/c$ structure of $LiGaH_4$.

constants, cell volumes, and atomic coordinates for the seven lowest-energy structures we have identified and indicates favorable overall comparison with both experiment and the results of Ref. 8.

All the $AGaH_4$ compounds are ionic insulators comprising A^{+1} ions and covalently bonded tetrahedral $(GaH_4)^{-1}$ complexes having the particularly stable configuration of 18 valence electrons. The Ga-H distances d(Ga-H) are $\cong$1.6 Å throughout the series and most of the H-Ga-H bond angles are very near the 109.5° value characterizing a regular tetrahedron, as Table II shows. With this atomic arrangement the cell volume V can be expected to vary linearly with the volume of the alkali ion. Figure 1 plots V against r_A^3, where r_A is the radius of the A^{+1} ion (r_A=0.68, 0.97, 1.33, 1.47, 1.67 Å for Li, Na, K, Rb, and Cs, respectively[41]), and demonstrates this to be the case. The calculated band gaps E_g, also included in Table II, are in the 4.5–5.0 eV range, increasing through the series. We emphasize that band gaps calculated via standard density functional theory are generally smaller than experimental values; however, the trend within a series of compounds is expected to be well represented.

In the absence of experimental information we cannot distinguish the two $LiGaH_4$ structures, which have nearly identical cell volumes and atomic arrangements as well as electronic and vibrational energies. Their calculated x-ray powder diffraction diagrams (Fig. 2) are distinct, however, so that diffraction measurements should be able to straightforwardly determine if either of them is the actual ground-state configuration.

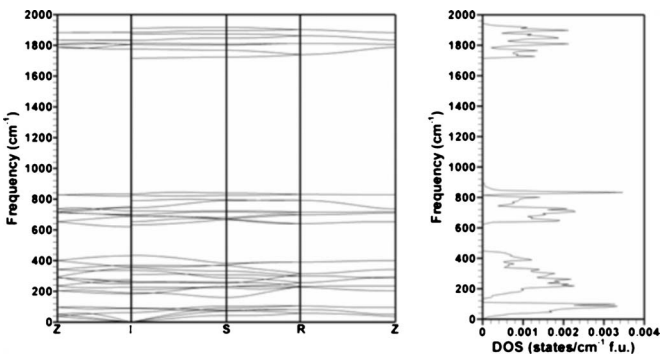

FIG. 4. Phonon spectrum and corresponding DOS for the orthorhombic *Cmcm* structure of $LiGaH_4$.

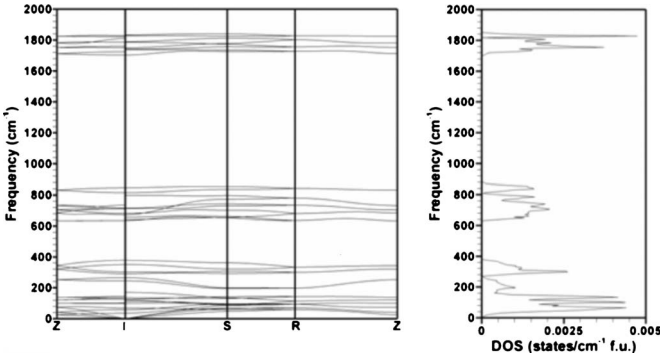

FIG. 5. Phonon spectrum and corresponding DOS for the orthorhombic *Cmcm* structure of $NaGaH_4$.

Since the *Pnma* $CsGaH_4$ structure is observed,[31,33] we infer that the isoenergetic $P4_2/nmc$ structure is simply a good approximation to it and not another phase that may exist at higher temperature and/or pressure. We include it here to emphasize the point that DFT calculations for a suite of candidate structures may not be sufficient to identify the true ground-state structure in the absence of observational data. The fact that the *Pnma* structure has a ~4% lower volume implies more efficient packing and is a suggestive discriminator but it is not conclusive. The two structures have very different calculated diffraction patterns.

IV. DIELECTRIC PROPERTIES, PHONON SPECTRA, AND ZERO-POINT ENERGIES

As mentioned in Sec. II, displacements of atoms in a polar crystal may generate a macroscopic electric field that can impact other properties, phonon dispersion in particular. The field can raise the LO modes above the unaffected TO modes in the vicinity of the Γ-point. Knowledge of the high-frequency dielectric tensor and the BECT enables calculation of the splittings via the method of Pick *et al.*[25] We calculate dielectric tensors and the BECT using density functional perturbation theory[42] as recently implemented in the VASP code.[43] In this approach the tensor components are obtained by calculating the first-order response of the wave functions to an external electric field and to displacements of the ions. The change in the wave functions is cast directly into a cell-

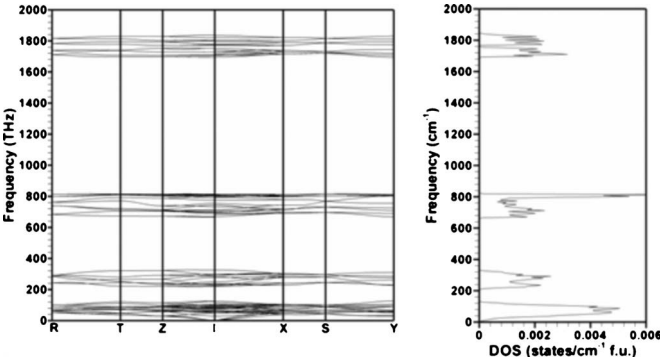

FIG. 6. Phonon spectrum and corresponding DOS for the orthorhombic *Pnma* structure of $KGaH_4$.

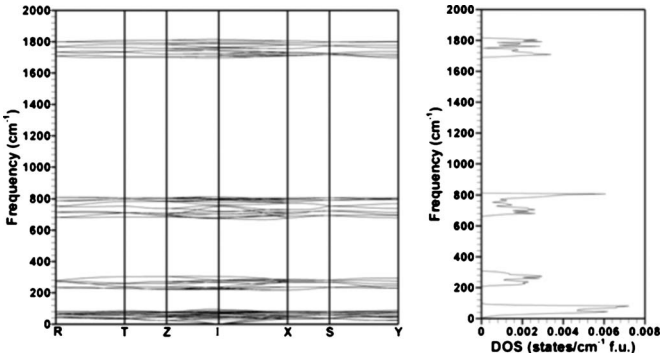

FIG. 7. Phonon spectrum and corresponding DOS for the orthorhombic *Pnma* structure of $RbGaH_4$.

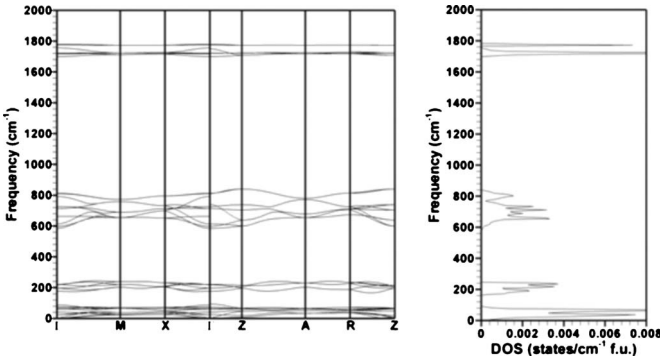

FIG. 9. Phonon spectrum and corresponding DOS for the tetragonal $P4_2/nmc$ structure of $CsGaH_4$.

periodic first-order change in the Hamiltonian. Tensor components are obtained by solving the resulting equations for directions corresponding to the principal axes.

Components of the high-frequency dielectric tensor $\varepsilon_{\alpha\beta}(\infty)$ (α,β denoting Cartesian directions) for the $AGaH_4$ hydrides are given in Table III. For the sake of comparison the components of the static (zero-frequency) dielectric tensor $\varepsilon_{\alpha\beta}(0)$ are listed as well, although only $\varepsilon_{\alpha\beta}(\infty)$ is required to calculate the LO/TO mode splittings. For each hydride the diagonal elements $\varepsilon_{\alpha\alpha}(\infty)$ are nearly equal, differing by less than 6%; the corresponding excursions are somewhat more pronounced for $\varepsilon_{\alpha\alpha}(0)$.

Tables IV–VI present our results for the BECT, designated as $Z^*_{\tau,\alpha\beta}$, where τ specifies a particular ion, α,β are Cartesian directions, and we denote the formal valence of atom τ as Z_τ. It is clear from the tables that the diagonal BECT components $Z^*_{A,\alpha\alpha}$ are near $Z_A=+1$ for the alkali-metal ions. On the other hand, $Z^*_{Ga,\alpha\alpha}$ and $Z^*_{H,\alpha\alpha}$ depart substantially from the formal valences $Z_{Ga}=+3$ and $Z_H=-1$, reflecting the covalent nature of the $(GaH_4)^{-1}$ molecular complexes.

Phonon spectra including the LO/TO mode splittings and corresponding densities of states are displayed in Figs. 3–9 for the seven $AGaH_4$ structures having the lowest total electronic energies. No soft modes or other anomalies occur in any of the dispersion relations: each structure is vibrationally stable. The LO/TO splittings near the Γ-point are most pronounced for $LiGaH_4$ (Figs. 3 and 4) and decrease with increasing mass of the A^{+1} ion. The spectra exhibit common qualitative features with even greater similarity among those sharing the same space-group symmetry (*Cmcm* in Figs. 4 and 5; *Pnma* in Figs. 6–8). The densities of states indicate four principal groups of vibrational modes across the series. Analysis of the corresponding ionic motions indicates that whole lattice vibrational modes of various types are contained in the 0–200 cm^{-1} interval. The modes with energies from 200–500 cm^{-1} are rocking oscillations of rigid $(GaH_4)^{-1}$ tetrahedra with unchanged Ga-H bond lengths and H-Ga-H bond angles while the 600–900 cm^{-1} and 1600–1900 cm^{-1} ranges comprise deformation and stretching modes of Ga-H pairs in the $(GaH_4)^{-1}$ molecular complexes, respectively. Our results can be compared with infra-

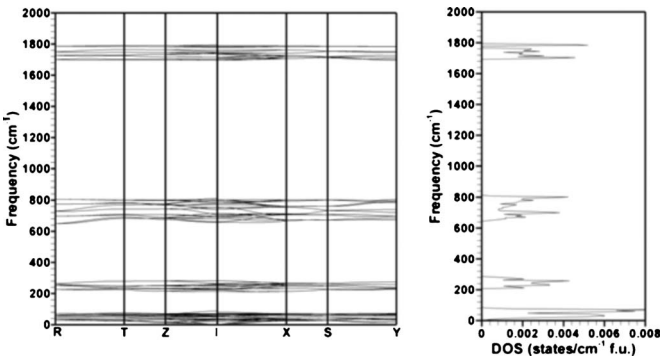

FIG. 8. Phonon spectrum and corresponding DOS for the orthorhombic *Pnma* structure of $CsGaH_4$.

TABLE VII. Calculated zero-point energies per stated formula unit (f.u.) of the material listed in the first column.

	Zero-point energy	
Material	meV/f.u.	kJ/mole f.u.
$LiGaH_4$ ($P2_1/c$)	811.8	78.33
$LiGaH_4$ (*Cmcm*)	802.1	77.39
$NaGaH_4$ (*Cmcm*)	758.3	73.16
$KGaH_4$ (*Pnma*)	748.6	72.23
$RbGaH_4$ (*Pnma*)	736.6	71.07
$CsGaH_4$ (*Pnma*)	723.8	69.84
$CsGaH_4$ ($P4_2/nmc$)	709.3	68.44
Li metal	47.8	4.61
Na metal	24.0	2.32
K metal	9.3	0.90
Rb metal	5.7	0.55
Cs metal	7.0	0.68
Ga metal	21.9	2.11
H_2 molecule	272.7	26.31
LiGa	76.8	7.41
LiH	225.6	21.77
NaH	157.5	15.20
KH	123.1	11.88
RbH	110.1	10.62
CsH	98.2	9.48

TABLE VIII. Room-temperature enthalpy of formation ΔH_{298} and its components for $A\mathrm{GaH_4}$ hydrides. All values in kilojoule per mole H_2.

	$LiGaH_4$ ($P2_1/c$)	$LiGaH_4$ ($Cmcm$)	$NaGaH_4$ ($Cmcm$)	$KGaH_4$ ($Pnma$)	$RbGaH_4$ ($Pnma$)	$CsGaH_4$ ($Pnma$)	$CsGaH_4$ ($P4_2/nmc$)
ΔH_{el}	−31.7	−31.8	−33.6	−56.0	−58.8	−64.0	−63.9
ΔH_{ZPE}	9.5	9.0	8.1	8.3	7.9	7.2	6.5
ΔH_0	−22.2	−22.8	−25.5	−47.7	−50.9	−56.8	−57.4
$\delta\Delta H_{298}$	−6.3	−6.1	−5.8	−6.1	−6.0	−5.6	−5.4
ΔH_{298}	−28.5	−28.8	−31.2	−53.8	−56.9	−62.4	−62.8

red and Raman experiments on the Na, K, Rb, and Cs hydrides reported by Kurbakova *et al.*[44] For $KGaH_4$, $RbGaH_4$, and $CsGaH_4$ broad structures with maxima near 1720, 1770, and 1800 cm^{-1} are identified as Ga-H stretch vibrations, and another set of broad structures with maxima near 710, 760, and 830 cm^{-1} are ascribed to Ga-H deformation modes. The spectra for $NaGaH_4$ are more complex with peaks shifted to higher energy by 40–80 cm^{-1}. Our calculated phonon spectra in Figs. 5–8 are in excellent quantitative agreement with the measured energies.[44]

Table VII lists the ZPEs emerging from our phonon calculations. Each ZPE is given by $\frac{1}{2}\Sigma_{\vec{q}}\hbar\omega_{\vec{q}}$, where $\omega_{\vec{q}}$ is the phonon frequency at wave vector $\vec{q}$. Even on a per H_2 basis the ZPEs of the $A\mathrm{GaH_4}$ hydrides are much larger than that of the isolated hydrogen molecule, evidently reflecting substantial zero-point motion of the $(GaH_4)^{-1}$ complexes. Unsurprisingly, the ZPEs of the two $LiGaH_4$ and the two $CsGaH_4$ structures are very similar, differing by only 1% and 2%, respectively.

V. ENTHALPIES OF FORMATION

We write the standard enthalpy of formation ΔH_T corresponding to the reaction

$$A + \mathrm{Ga} + 2\mathrm{H_2} \leftrightarrow A\mathrm{GaH_4} \tag{1}$$

at temperature T as

$$\Delta H_T = \Delta H_0 + \delta\Delta H_T. \tag{2}$$

The $T=0$ value ΔH_0 is the sum of the electronic and ZPE components,

$$\Delta H_0(A\mathrm{GaH_4}) = \Delta H_{el} + \Delta H_{ZPE} = [E_{el}(A\mathrm{GaH_4}) - E_{el}(A) - E_{el}(\mathrm{Ga}) - 2E_{el}(\mathrm{H_2})] + [E_{ZPE}(A\mathrm{GaH_4}) - E_{ZPE}(A) - E_{ZPE}(\mathrm{Ga}) - 2E_{ZPE}(\mathrm{H_2})] \tag{3}$$

and the finite T contribution is specified by

$$\delta\Delta H_T(A\mathrm{GaH_4}) = E_{ph}(A\mathrm{GaH_4}) - E_{ph}(A) - E_{ph}(\mathrm{Ga}) - 2\left[\frac{7}{2}kT + E_{vib}(\mathrm{H_2})\right], \tag{4}$$

where $E_{ph}=\Sigma_{\vec{q}}\hbar\omega_{\vec{q}}n(\omega_{\vec{q}})$ with $n(\omega)=(e^{\hbar\omega/kT}-1)^{-1}$ is the phonon energy without the ZPE, $\frac{7}{2}kT$ comprises the translational ($\frac{3}{2}kT$), rotational (kT), and $pV=kT$ energies of the H_2 molecule, and $E_{vib}=\hbar\omega_0 n(\omega_0)$ is the H_2 vibrational energy. pV for the A and Ga metals is ignored since their small molar volumes make pV insignificant at $p=1$ bar. Table VIII presents the room-temperature formation enthalpy ΔH_{298} and its components. We note that even with the inclusion of the phonon terms (ZPEs and finite-temperature contributions) the two $LiGaH_4$ and two $CsGaH_4$ remain energetically indistinguishable.

$LiGaH_4$ and $NaGaH_4$ are the most interesting $A\mathrm{GaH_4}$ materials from the perspective of hydrogen storage. They have the largest hydrogen gravimetric densities, which are 5.0%, 4.2%, 3.6%, 2.5%, and 2.0% for the A=Li, Na, K, Rb, and Cs members of the series, respectively. Moreover, as Table VIII shows, both feature $\Delta H_{298}\sim -30$ kJ/mole H_2, a value for which the van't Hoff relation,

$$\ln P\ (\mathrm{bar}) = \Delta H/RT - \Delta S/R \tag{5}$$

implies an equilibrium temperature T (1 bar) near room temperature for a hydrogen pressure P of 1 bar (with the reasonable assumption that the entropy change ΔS is roughly that of H_2 gas, ~130 J/K mole H_2).

To our knowledge no measurements of ΔH_{298} are available. Measured values of $(H_{298}-H_0)$ and the entropy S_{298} at 298 K, however, have been reported by Gavrichev[45] for the Na, K, Rb, and Cs hydrides. The corresponding quantities derived from our calculated phonon spectra are E_{ph} and

$$S_T = k\sum_{\vec{q}}\left[\ln\left(2\ \mathrm{csch}\frac{1}{2}x\right) + \frac{1}{2}x\ \coth\frac{1}{2}x\right], \tag{6}$$

where $x\equiv\hbar\omega_{\vec{q}}/kT$. Table IX demonstrates very favorable comparison between experiment and theory, indicating that phonon excitation is primarily responsible for the temperature dependence of the $A\mathrm{GaH_4}$ enthalpy and entropy.

TABLE IX. Enthalpy change $(H_{298}-H_0)$ and entropy S_{298} of $A\mathrm{GaH_4}$ hydrides.

Hydride (space group)	$H_{298}-H_0$ (kJ/mole H_2)		S_{298} (J/K mole H_2)	
	Expt.[a]	Theory	Expt.[a]	Theory
$NaGaH_4$ ($Cmcm$)	8.885	8.368	61.300	60.382
$KGaH_4$ ($Pnma$)	8.660	8.646	62.200	65.600
$RbGaH_4$ ($Pnma$)	9.195	8.950	69.200	71.444
$CsGaH_4$ ($Pnma$)	9.450	9.208	74.100	77.381

[a]Reference 43.

TABLE X. Calculated C_{ij}; polycrystalline moduli B_{VRH}, G_{VRH}, B_{VRH}; and Debye temperature Θ of monoclinic $LiGaH_4$. All C_{ij} and moduli in gigapascal.

$LiGaH_4$ ($P2_1/c$)			
C_{11}	21.6	C_{44}	8.8
C_{12}	5.8	C_{46}	−0.7
C_{13}	10.4	C_{55}	9.4
C_{15}	−1.5	C_{66}	10.1
C_{22}	29.5	B_{VRH}	13.8
C_{23}	8.9	G_{VRH}	8.9
C_{25}	−1.0	Y_{VRH}	21.9
C_{33}	25.4	Θ (K)	304
C_{35}	−3.0		

Returning to Table VIII, we emphasize that the ΔH values apply to reaction (1) in which $AGaH_4$ forms from its individual elemental constituents. From a technological standpoint the reaction

$$AGa + 2H_2 \leftrightarrow AGaH_4 \tag{7}$$

is preferable since it involves two solid phases instead of three as well as the likelihood of concomitantly less transport of A and Ga. Unfortunately, LiGa is the only AGa binary for which there is definitive structural information.[46] It has the Zintl fcc NaTl-type structure ($Fd\bar{3}m$; space group No. 227). Optimizing that structure with VASP and computing the phonon spectrum (which exhibits no anomalies), we find that the enthalpy corresponding to reaction (7) is

$$\begin{aligned}\Delta H_{\mathrm{R}}(\mathrm{LiGa}) \equiv \Delta H_{\mathrm{el}} + \Delta H_{\mathrm{ZPE}} + \delta\Delta H_{298} &= [E_{\mathrm{el}}(\mathrm{LiGaH_4}) \\ &- E_{\mathrm{el}}(\mathrm{LiGa}) - 2E_{\mathrm{el}}(\mathrm{H_2})] + [E_{\mathrm{ZPE}}(\mathrm{LiGaH_4}) \\ &- E_{\mathrm{ZPE}}(\mathrm{LiGa}) - 2E_{\mathrm{ZPE}}(\mathrm{H_2})] + \left[E_{\mathrm{ph}}(\mathrm{LiGaH_4}) \right. \\ &\left. - E_{\mathrm{ph}}(\mathrm{LiGa}) - 2\left[\frac{7}{2}kT + E_{\mathrm{vib}}(\mathrm{H_2})\right]\right] \\ &= 3.2(3.5)\ \mathrm{kJ/mole\ H_2}\end{aligned} \tag{8}$$

for the $Cmcm$ ($P2_1/c$) $LiGaH_4$ structure in Table I.

Since the binary alkali hydrides AH are quite stable materials, we also evaluate the enthalpy $\Delta H_{\mathrm{R}}(A\mathrm{H})$ for the reaction

$$A\mathrm{H} + \mathrm{Ga} + (3/2)\mathrm{H_2} \leftrightarrow A\mathrm{GaH_4}: \tag{9}$$

$$\begin{aligned}\Delta H_{\mathrm{R}}(A\mathrm{H}) \equiv [E_{\mathrm{el}}(A\mathrm{GaH_4}) &- E_{\mathrm{el}}(A\mathrm{H}) - E(\mathrm{Ga}) - (3/2)E_{\mathrm{el}}(\mathrm{H_2})] \\ &+ [E_{\mathrm{ZPE}}(A\mathrm{GaH_4}) - E_{\mathrm{ZPE}}(A\mathrm{H}) - E_{\mathrm{ZPE}}(\mathrm{Ga}) \\ &- (3/2)E_{\mathrm{ZPE}}(\mathrm{H_2})] + \left[E_{\mathrm{ph}}(A\mathrm{GaH_4}) - E_{\mathrm{ph}}(A\mathrm{H}) \right. \\ &\left. - E_{\mathrm{ph}}(\mathrm{Ga}) - (3/2)\left[\frac{7}{2}kT + E_{\mathrm{vib}}(\mathrm{H_2})\right]\right].\end{aligned} \tag{10}$$

Phonon calculations were done for each AH, all of which crystallize in the fcc $Fm\bar{3}m$ rocksalt structure, to obtain the ZPEs (included in Table VII) and E_{ph} terms. We find $\Delta H_{\mathrm{R}}(A\mathrm{H}) = 13.3(13.7)$; −8.3; −30.2; −36.2; −41.5 (−41.9) kJ/mole H_2 for $Cmcm$ ($P2_1/c$) $LiGaH_4$, $CmCm$ $NaGaH_4$, $Pnma$ $KGaH_4$, $Pnma$ $RbGaH_4$, and $Pnma$ ($P4_2/nmc$) $CsGaH_4$, respectively. Thus, $LiGaH_4$ is the only $AGaH_4$ compound predicted to be thermodynamically un-

TABLE XI. Calculated C_{ij}; polycrystalline moduli B_{VRH}, G_{VRH}, B_{VRH}; and Debye temperature Θ of $AGaH_4$ hydrides calculated in this work. Theoretical single-crystal bulk moduli B_0 are from Ref. 8. All C_{ij} and moduli in gigapascal.

					$CsGaH_4$	
	$LiGaH_4$ ($Cmcm$)	$NaGaH_4$ ($Cmcm$)	$KGaH_4$ ($Pnma$)	$RbGaH_4$ ($Pnma$)	($Pnma$)	($P4_2/nmc$)
C_{11}	46.8	26.5	18.7	17.0	14.7	14.3
C_{12}	4.6	7.1	9.6	9.2	8.7	5.9
C_{13}	8.8	2.6	5.3	4.2	3.5	0.8
C_{22}	14.5	29.5	17.0	15.7	12.6	$=C_{11}$
C_{23}	5.9	7.4	5.1	3.6	4.3	
C_{33}	34.4	32.2	20.5	20.9	15.7	21.0
C_{44}	13.0	9.2	5.0	5.1	4.7	2.9
C_{55}	10.4	3.5	5.0	5.0	2.7	7.6
C_{66}	10.5	8.5	8.8	9.0	8.2	
B_{VRH}	13.2	13.5	10.7	9.7	8.4	7.2
B_0 [a]	11.97	13.19	10.15	9.41	8.22	
G_{VRH}	11.2	8.2	5.9	5.9	4.4	4.9
Y_{VRH}	26.2	20.3	15.0	14.7	11.2	11.9
Θ (K)	337	273	222	189	147	154

[a]Reference 8.

stable with respect to *A*H, Ga metal, and H_2 gas. Assuming our $LiGaH_4$ structures lead to sufficiently accurate energies, we suggest that the thermodynamic instability of $LiGaH_4$ against LiGa [$\Delta H_R(\text{LiGa}) > 0$ from Eq. (8)] and LiH [$\Delta H_R(\text{LiH}) > 0$ from Eq. (10)] formation provides an explanation for the difficulty of its synthesis.

VI. ELASTIC CONSTANTS AND ELASTIC STABILITY

Information on elastic behavior is of fundamental interest for materials in general, and it may hold particular value for understanding the response of hydrides subjected to mechanical stress. Baldi *et al.*,[47] for example, recently demonstrated that the thermodynamic stability of the Mg-H system can be modified dramatically by elastic constraints.

Single-crystal elastic constants C_{ij} calculated for the seven energetically most favorable $AGaH_4$ structures are reported in Tables X and XI. Voigt-Reuss-Hill estimates B_{VRH}, G_{VRH}, and Y_{VRH} of the polycrystalline bulk (B), shear (G), and Young's (Y) moduli computed from the C_{ij}, and the Debye temperature Θ estimated from them in turn (following the procedures detailed in Ref. 27), are also presented in these tables. Vajeeston *et al.*[8] derived single crystal bulk moduli B_0 from their calculated $E(V)$ curves, and Table XI indicates that those agree well with our B_{VRH} results; the largest departure is 9% for *Cmcm* $LiGaH_4$. No measured values of the quantities in Tables X and XI are available in the literature. With B_{VRH} values in the 13–8 GPa range through the series, the $AGaH_4$ hydrides are substantially more compressible than their *A*H alkali hydride cognates, whose bulk moduli vary from ~34 GPa for LiH to ~10 GPa for CsH.[48]

We examined the mechanical stability of each hydride in Tables X and XI by diagonalizing the C_{ij} tensor and evaluating the Born stability criteria.[49] For every material we find that all six eigenvalues of C_{ij} are positive, confirming mechanical stability in the absence of applied stress (as discussed, for example, in Ref. 50). This is consistent with the fact that the $\omega_{\vec{q}} \rightarrow 0$ acoustic branches at the Γ-point in the phonon spectra of Figs. 3–9 all have positive slopes.

VII. SUMMARY

We have explored systematic aspects of the $AGaH_4$ hydride series with DFT. Two candidate crystal structures have been identified for the unknown structure of $LiGaH_4$. Dielectric properties, including the static and high-frequency dielectric tensors and the Born effective charge tensor, phonon dispersion relations, formation enthalpies, and all independent elasticity tensor components have been calculated. $LiGaH_4$ and $NaGaH_4$ especially merit experimental inquiry in view of their substantial gravimetric hydrogen density and attractive standard enthalpy of formation. Our finding that $LiGaH_4$ is thermodynamically unstable with respect to both LiGa and LiH, and the fact that no NaGa binary exists, however, make the prospect of their enjoying significant practical utility as hydrogen storage materials problematic.

ACKNOWLEDGMENTS

We appreciate illuminating and helpful discussions with K. S. Gavrichev, G. P. Meisner, F. E. Pinkerton, and P. Saxe. Computational resources, networking, and support were provided by GM Information Systems and Services.

[1] B. Bogdanović and M. Schwickardi, J. Alloys Compd. **253-254**, 1 (1997).
[2] G. P. Meisner, G. G. Tibbetts, F. E. Pinkerton, C. H. Olk, and M. P. Balogh, J. Alloys Compd. **337**, 254 (2002).
[3] A. Züttel,S. Rentsch, P. Fischer, P. Wemger, P. Sudan, Ph. Mauron, Ch. Emmenegger, J. Alloys Compd. **356-357**, 515 (2003).
[4] O. M. Løvvik, S. M. Opalka, H. W. Brinks, and B. C. Hauback, Phys. Rev. B **69**, 134117 (2004).
[5] J. F. Mao, X. B. Yu, Z. P. Guo, C. K. Poh, H. K. Liu, Z. Wu, and J. Ni, J. Phys. Chem. C **113**, 10813 (2009).
[6] A. Peles and C. G. Van de Walle, Phys. Rev. B **76**, 214101 (2007).
[7] L. G. Hector, Jr., J. F. Herbst, W. Wolf, P. Saxe, and G. Kresse, Phys. Rev. B **76**, 014121 (2007).
[8] P. Vajeeston, P. Ravindran, R. Vidya, H. Fjellvåg, and A. Kjekshus, Cryst. Growth Des. **4**, 471 (2004).
[9] L. G. Hector, Jr. and J. F. Herbst, J. Phys.: Condens. Matter **20**, 064229 (2008).
[10] W. Kohn and L. Sham, Phys. Rev. **140**, A1133 (1965).
[11] G. Kresse and J. Hafner, Phys. Rev. B **49**, 14251 (1994).
[12] G. Kresse and J. Furthmüller, Comput. Mater. Sci. **6**, 15 (1996).
[13] P. E. Blöchl, Phys. Rev. B **50**, 17953 (1994).
[14] G. Kresse and D. Joubert, Phys. Rev. B **59**, 1758 (1999).
[15] J. P. Perdew and Y. Wang, Phys. Rev. B **45**, 13244 (1992).
[16] J. P. Perdew, J. A. Chevary, S. H. Vosko, K. A. Jackson, M. R. Pederson, D. J. Singh, and C. Fiolhais, Phys. Rev. B **46**, 6671 (1992).
[17] S. H. Vosko, L. Wilk, and M. Nusair, Can. J. Phys. **58**, 1200 (1980).
[18] W. H. Press, S. A. Teukolsky, W. T. Vetterling, and B. P. Flannery, *Numerical Recipes in FORTRAN 90: The Art of Parallel Scientific Computing*, 2nd ed. (Cambridge University Press, New York, 1996).
[19] H. J. Monkhorst and J. D. Pack, Phys. Rev. B **13**, 5188 (1976).
[20] P. E. Blöchl, O. Jepsen, and O. K. Anderson, Phys. Rev. B **49**, 16223 (1994).
[21] K. Parlinski, Software PHONON 4.30, Cracow, as implemented in MEDEA 2.4, Materials Design, Le Mans, France and Angel Fire, (NM) USA, www.MaterialsDesign.com
[22] G. Kresse, J. Furthmüller, and J. Hafner, Europhys. Lett. **32**, 729 (1995).
[23] K. Parlinski, Z. Q. Li, and Y. Kawazoe, Phys. Rev. Lett. **78**, 4063 (1997).
[24] M. Methfessel and A. T. Paxton, Phys. Rev. B **40**, 3616 (1989).
[25] R. M. Pick, M. H. Cohen, and R. M. Martin, Phys. Rev. B **1**, 910 (1970).
[26] Y. Le Page and P. Saxe, Phys. Rev. B **65**, 104104 (2002).
[27] L. G. Hector, Jr., J. F. Herbst, and T. W. Capehart, J. Alloys

Compd. **353**, 74 (2003).
[28] L. G. Hector, Jr. and J. F. Herbst, J. Alloys Compd. **379**, 41 (2004).
[29] R. Stadler, W. Wolf, R. Podloucky, G. Kresse, J. Furthmüller, and J. Hafner, Phys. Rev. B **54**, 1729 (1996).
[30] A. V. Irodova, V. A. Somenkov, S. I. Bakum, and S. F. Kuznetsova, Z. Phys. Chem., Neue Folge **163**, S239 (1989).
[31] L. M. Kovba, V. E. Gorbunov, and K. S. Gavrichev, Russ. J. Inorg. Chem. **31**, 148 (1986).
[32] Yu. Z. Nozik, E. S. Kuklina, N. A. Bliznyuk, and S. V. Borisov, Kristallografiya **36**, 57 (1991).
[33] T. N. Dymova and Yu. M. Dergachev, Bull. Acad. Sci. USSR, Div. Chem. Sci. **30**, 935 (1981).
[34] A. E. Finholt, A. C. Bond, Jr., and H. I. Schlesinger, J. Am. Chem. Soc. **69**, 1199 (1947).
[35] S. I. Bakum and S. F. Ereshko, Russ. J. Inorg. Chem. **22**, 360 (1977).
[36] P. Fischer and A. Züttel, Paul Scherrer Institute Annual Reports. Available from http://num.web.psi.ch/reports/2001/pdf/g09.pdf
[37] P. Fischer and A. Züttel, Mater. Sci. Forum **443-444**, 287 (2004).
[38] T. Mueller and G. Ceder, Phys. Rev. B **74**, 134104 (2006).
[39] E. H. Majzoub and V. Ozolins, Phys. Rev. B **77**, 104115 (2008).
[40] A. R. Oganov and C. W. Glass, J. Phys.: Condens. Matter **20**, 064210 (2008).
[41] *CRC Handbook of Chemistry and Physics*, 67th ed. (CRC Press, Boca Raton, FL, 1986).
[42] S. Baroni and R. Resta, Phys. Rev. B **33**, 7017 (1986).
[43] M. Gajdoš, K. Hummer, G. Kresse, J. Furthmüller, and F. Bechstedt, Phys. Rev. B **73**, 045112 (2006).
[44] A. P. Kurbakova, L. A. Leites, V. V. Gavrilenko, Yu. N. Karaksin, and L. I. Zakharkin, Spectrochim. Acta, Part A **31**, 281 (1975).
[45] K. S. Gavrichev, Inorg. Mater. **39**, S89 (2003).
[46] Reference 33 contains speculative mention of a CsGa binary with the $Fd\bar{3}m$ NaTl-type structure. Our calculations indicate, however, that it is thermodynamically unfavorable with respect to its constituent elements (positive standard enthalpy of formation ΔH) as well as elastically and vibrationally unstable. Via a search for other candidates we identified an orthorhombic *Cmca* (No. 64) KTl-type CsGa structure that has a negative ΔH (and lowest of those investigated), is elastically stable, and whose phonon spectrum contains no anomalies. This structure is thermodynamically unstable, however, against decomposition to Cs metal and the known Cs_8Ga_{11} phase, which is consistent with the absence of a CsGa binary in the available Cs-Ga phase diagrams.
[47] A. Baldi, M. Gonzalez-Silveira, V. Palmisano, B. Dam, and R. Griessen, Phys. Rev. Lett. **102**, 226102 (2009).
[48] N. Novaković, I. Radisavljević, D. Colognesi, S. Ostojić, and N. Ivanović, J. Phys.: Condens. Matter **19**, 406211 (2007).
[49] M. Born and H. Huang, *Dynamical Theory of Crystal Lattices* (Clarendon Press, Oxford, 1954).
[50] S. Yip, J. Li, M. Tang, and J. Wang, Mater. Sci. Eng., A **317**, 236 (2001).